Progress In Electromagnetics Research, PIER 74, 195–216, 2007

ANALYSIS OF TWO-DIMENSIONAL MAGNETO-DIELECTRIC GRATING SLAB

A. M. Attiya

Electronics Research Institute (ERI)
El-Tahreer St., Dokki, Giza, 12622, Egypt

A. A. Kishk and A. W. Glisson

Department of Electrical Engineering
Center of Applied Electromagnetic System Research (CAESR)
University of Mississippi
University, MS 38677, USA

Abstract—Vectorial modal analysis of a 2-D magneto-dielectric grating structure is presented. The modal analysis is combined with the generalized scattering matrix to obtain the transmission and reflection coefficients of multilayered 2-D magneto-dielectric grating slabs. The results are verified with available commercial codes. Physical interpretation of the grating slab behavior is introduced. An equivalent homogeneous magneto-dielectric slab is found using a simple approach for extracting the equivalent permittivity and permeability. Several examples are presented to find the relation between the physical parameters of magneto-dielectric grating slabs and their equivalent parameters. Emphasis on the possibility of designing a metamaterial with equivalent negative permittivity and/or negative permeability by using these grating structures is considered.

1. INTRODUCTION

Periodic structures have found great interests in different electromagnetic and optical applications. This was the motivation to develop different techniques for studying different configurations of periodic structures. However, only a few published works have discussed the properties of magneto-dielectric periodic structures [1, 2]. Recently, it has been shown that such magneto-dielectric periodic structures can also be used to design double negative (DNG) metamaterial where both

the relative permittivity and the relative permeability are negative values [3]. Such metamaterials with negative permittivity and/or negative permeability have found important applications in focusing the fields of low directivity antennas [4, 5]. However, the available study for designing metamaterial based on a periodic magneto-dielectric structure is based on analytical forms for a special case where the structure is composed of spherical magneto-dielectric spheres arranged in three-dimensional (3D) cubic cells [3]. For practical applications, it would be more appropriate to study the possibility of realizing such metamaterials by using a 2-D grating slab of finite thickness as shown in Fig. 1. In addition, including the relative permeability as a design parameter represents another degree of freedom for designing grating structures.

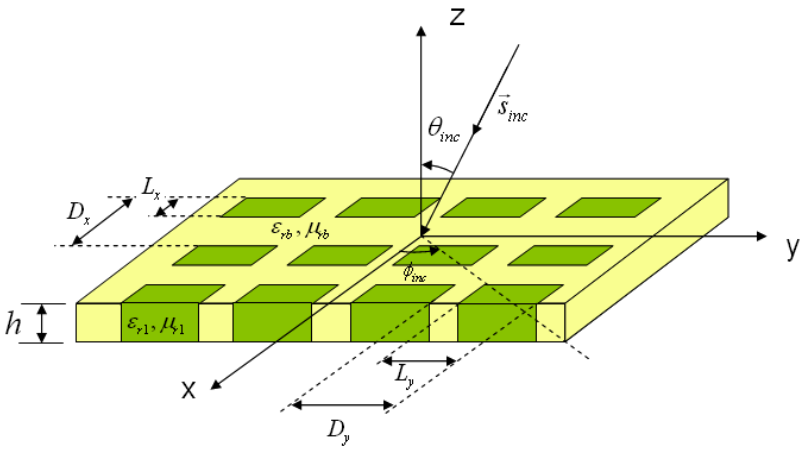

Figure 1. Geometry of a 2-D Magneto-dielectric grating slab.

From the analytical point of view, the problem of a magneto-dielectric grating slab can be solved by using different techniques; such as MoM, FDTD, FDFD, FEM, and modal analysis [1, 2, 6–12]. This problem has been discussed previously by using MoM [1, 2]. However, the main complexity of this method is the large number of expansion functions that are required to represent the induced volume electric and magnetic currents. This complexity also increases by increasing the thickness of the slab. Unlike MoM, modal analysis is based on obtaining the tangential field distributions of the different modes and the corresponding propagation constants in the longitudinal directions. Then the problem is treated as cascaded sections of guiding structures by using the generalized scattering method [13]. In this case, the complexity of the problem is independent of the thickness of the grating structure. Coves et al. [8, 9] applied this modal analysis to study

the reflection and transmission of 1-D dielectric grating structures. They showed good agreement with other techniques and experimental results. They also showed good convergence and flexibility in their modal analysis to include complex dielectric permittivity. Another advantage of this technique is that the required integrations can be calculated analytically for simple shapes of the implanted rods. Attiya and Kishk [17] generalized this modal analysis method to study 2-D dielectric grating slab. This paper presents an additional generalization to include also the effect of changing the relative permeability on the characteristics of a 2-D magneto-dielectric grating slab.

The remaining problem is how to extract the equivalent parameters of the grating slab by using its reflection and transmission coefficients. Cheng and Ziolkowski [14] have obtained approximate formulas for such a problem based on the equivalent T-network. However, their approximation is limited to normal incidence and very thin thicknesses. Such an approximation was not found to be suitable for the structures proposed in this article. Thus, the problem is formulated as an inverse problem where the equivalent parameters are obtained by a simple optimization process. The objective for this optimization is to find the equivalent parameters that minimize the difference between the actual reflection and transmission coefficients and the corresponding ones for a homogeneous slab of the same thickness excited by the same incident field.

The following section presents the modal analysis of a 2-D magneto-dielectric grating structure and how it can be used to obtain the transmission and reflection coefficients of multilayered grating slabs. Then the problem of extracting equivalent parameters is discussed in Section 3. Section 4 presents sample results for different magneto-dielectric grating slabs and their equivalent parameters. This section presents also detailed discussions on the possibility of designing metamaterials by using magneto-dielectric grating slabs.

2. MODAL ANALYSIS OF MAGNETO-DIELECTRIC GRATING

An infinite 2-D grating can be assumed as a guiding structure where the total field is a superposition of discrete modes. The transverse magnetic field distribution and propagation constants of these discrete modes can be obtained by solving the following eigenvalue problem:

$$L[\vec{h}_t] = \beta^2 \vec{h}_t \tag{1}$$

where the longitudinal dependence is assumed to $e^{-j\beta z}$, β is the propagation constant and $L[\circ]$ is a transverse differential operator.

For the case where both ε_r and μ_r are functions of the transverse coordinates, the transverse differential operator $L[\circ]$ can be derived by using Maxwell's equations as follows:

$$L[\circ] = \left[\nabla_t^2(\circ) + k_0^2\mu_r\varepsilon_r(\circ) + \left(\frac{\nabla_t\varepsilon_r}{\varepsilon_r}\right) \times (\nabla_t \times \circ) + \nabla_t\left(\frac{\nabla_t\mu_r}{\mu_r} \cdot \circ\right)\right] \tag{2}$$

To solve Eq. (1) numerically, the transverse magnetic field distribution can be approximated as a series of orthonormal expansion functions of unknown amplitudes as

$$\vec{h}_t = \vec{h}_t^{TE} + \vec{h}_t^{TM} = \sum_p C_{(p)}^{TE}\vec{\tilde{h}}_{(p)}^{TE} + C_{(p)}^{TM}\vec{\tilde{h}}_{(p)}^{TM} \tag{3}$$

where $\vec{\tilde{h}}_{(p)}^{TE}$ and $\vec{\tilde{h}}_{(p)}^{TM}$ are the TE and TM expansion functions of the pth mode and $C_{(p)}^{TE}$ and $C_{(p)}^{TM}$ are the corresponding unknown amplitudes of the expansion functions. Appropriate choices for these expansion functions for the case of a 2-D periodic structure in the transverse plane are

$$\vec{\tilde{h}}_{mn}^{TE} = \frac{\exp(-jk_{xm}x - jk_{yn}y)}{\sqrt{D_xD_y}}(\cos\phi_{inc}\vec{a}_x + \sin\phi_{inc}\vec{a}_y) \tag{4a}$$

$$\vec{\tilde{h}}_{mn}^{TM} = \frac{\exp(-jk_{xm}x - jk_{yn}y)}{\sqrt{D_xD_y}}(-\sin\phi_{inc}\vec{a}_x + \cos\phi_{inc}\vec{a}_y) \tag{4b}$$

where each mn combination corresponds to a particular mode in Eq. (3),

$$k_{xm} = k_{x0} + 2\pi m/D_x \tag{4c}$$

$$k_{yn} = k_{y0} + 2\pi n/D_y \tag{4d}$$

$$k_{x0} = k_0\sin\theta_{inc}\cos\phi_{inc} \tag{4e}$$

$$k_{y0} = k_0\sin\theta_{inc}\sin\phi_{inc} \tag{4f}$$

D_x and D_y are the dimensions of the periodic cell, and θ_{inc} and ϕ_{inc} correspond to the direction of incidence. The orthonormality relation can be easily verified for these expansion functions as follows

$$\left\langle \vec{\tilde{h}}_{mn}^{\zeta}, \vec{\tilde{h}}_{m'n'}^{\xi} \right\rangle = \int_0^{D_x}\int_0^{D_y} \vec{\tilde{h}}_{mn}^{\zeta^*} \cdot \vec{\tilde{h}}_{m'n'}^{\xi} dxdy = \delta_{mm'}\delta_{nn'}\delta_{\zeta\xi} \tag{5}$$

By applying Eq. (3) in Eq. (1) and using Galerkin's method, one can formulate the eigenvalue problem of Eq. (1) as a matrix eigenvalue

problem

$$\begin{bmatrix} \left[L_{pq}^{TE/TE}\right] & \left[L_{pq}^{TE/TM}\right] \\ \left[L_{pq}^{TM/TE}\right] & \left[L_{pq}^{TM/TM}\right] \end{bmatrix} \begin{bmatrix} \left[C_{(q)}^{TE}\right] \\ \left[C_{(q)}^{TM}\right] \end{bmatrix} = \beta^2 \begin{bmatrix} \left[C_{(q)}^{TE}\right] \\ \left[C_{(q)}^{TM}\right] \end{bmatrix} \tag{6}$$

where $L_{pq}^{\xi/\zeta} = \left\langle \vec{\tilde{h}}_{(p)}^{\xi}, L\left[\vec{\tilde{h}}_{(p)}^{\zeta}\right] \right\rangle$. By solving the above matrix eigenvalue problem, one can obtain the unknown amplitudes of the expansion functions for each mode as the eigenvectors and the propagation constants as the square roots of the corresponding eigenvalues. For the special case of a grating structure composed of rectangular dielectric rods, the matrix elements of Eq. (6) can be obtained in closed forms as shown in Appendix A. Other shapes of implanted rods can also be subdivided to several rectangular rods.

To obtain the reflection and transmission coefficients of the different modes between two adjacent semi-infinite gratings of the same periodicity, it is required to match the tangential electric and magnetic field distributions on the transverse interface between two grating structures. The tangential magnetic field distribution of each mode is obtained directly by using the resultant eigenvectors of Eq. (6). On the other hand, the transverse electric field distribution can be obtained as a function of the transverse magnetic field distribution as follows:

$$j\omega\varepsilon_0\varepsilon_r\vec{e}_t = \left[\nabla_t \times \vec{a}_z \left(-j\beta^{-1}\left(\mu_r^{-1}\nabla_t\mu_r \cdot \vec{h}_t + \nabla_t \cdot \vec{h}_t\right)\right) - j\beta\vec{a}_z \times \vec{h}_t\right] \tag{7}$$

This electric field distribution can also be approximated as a series of orthonormal expansion functions

$$\vec{e}_t = \vec{e}_t^{TE} + \vec{e}_t^{TM} = \sum_p \Phi_{(p)}^{TE}\vec{\tilde{e}}_{(p)}^{TE} + \Phi_{(p)}^{TM}\vec{\tilde{e}}_{(p)}^{TM} \tag{8}$$

where the expansion functions of the electric field are orthogonal to the corresponding expansion functions of the magnetic field such that $\vec{\tilde{e}}_{(p)}^{TE} = -\vec{a}_z \times \vec{\tilde{h}}_{(p)}^{TE}$ and $\vec{\tilde{e}}_{(p)}^{TM} = -\vec{a}_z \times \vec{\tilde{h}}_{(p)}^{TM}$. The electric field amplitude matrix Φ can be obtained by using the bi-orthogonal property of the electric field modal expansion function as follows:

$$j\omega\varepsilon_0\left\langle \vec{\tilde{e}}, \varepsilon_r, \vec{e}_t \right\rangle = \left\langle \vec{\tilde{e}}, \left[\left(-j\beta^{-1}C\left(\mu_r^{-1}\nabla_t\mu_r \cdot \vec{\tilde{h}}_t + \nabla_t \cdot \vec{\tilde{h}}_t\right)\right) - j\beta C\vec{a}_z \times \vec{\tilde{h}}_t\right] \right\rangle \tag{9}$$

By solving (9), it can be shown that the electric field amplitude matrix Φ is

$$\Phi = \frac{1}{j\omega\varepsilon_0}\left(j\beta^{-1}CQA^T - j\beta^{-1}CAA^T + j\beta C\right)\Psi^{-1} \tag{10}$$

where $A = \begin{bmatrix} A^{TE} \\ A^{TM} \end{bmatrix}$, $Q = \begin{bmatrix} Q^{TE} \\ Q^{TM} \end{bmatrix}$, and $\Psi = \begin{bmatrix} \Psi^{TE} & 0 \\ 0 & \Psi^{TM} \end{bmatrix}$. A^{TE} is a diagonal matrix with the elements $A^{TE}_{pp} = (-jk_{x(p)}\cos\phi_{inc} - jk_{y(p)}\sin\phi_{inc})$ and A^{TM} is a diagonal matrix with the elements $A^{TM}_{pp} = (jk_{x(p)}\sin\phi_{inc} - jk_{y(p)}\cos\phi_{inc})$. $\Psi^{TE} = \Psi^{TM}$ is a matrix with elements given as

$$\psi_{pq} = \frac{1}{D_x D_y}\int_0^{D_x}\int_0^{D_y} \varepsilon_r(x,y) e^{j(k_{x(p)}-k_{x(q)})x} e^{j(k_{y(p)}-k_{y(q)})y} dxdy \tag{11}$$

and the elements of the Q^{TE} and Q^{TM} matrices are

$$\begin{aligned} Q^{TE}_{pq} &= \Big(Q_{1x}\left(k_{x(p)} - k_{x(q)}, k_{y(p)} - k_{y(q)}\right)\cos\phi_{inc} \\ &\quad + Q_{1y}\left(k_{x(p)} - k_{x(q)}, k_{y(p)} - k_{y(q)}\right)\sin\phi_{inc}\Big) \qquad (12a) \\ Q^{TM}_{pq} &= \Big(-Q_{1x}\left(k_{x(p)} - k_{x(q)}, k_{y(p)} - k_{y(q)}\right)\sin\phi_{inc} \\ &\quad + Q_{1y}\left(k_{x(p)} - k_{x(q)}, k_{y(p)} - k_{y(q)}\right)\cos\phi_{inc}\Big) \qquad (12b) \end{aligned}$$

where Q_{1x} and Q_{1y} are given by Eqs. (A3e) and (A3f) in Appendix A.

By matching the tangential electric and magnetic fields on the interface between two adjacent semi-infinite 2-D grating structures of the same periodicity, one can obtain the corresponding scattering matrix elements

$$\begin{aligned} S_{11} &= I - 2\left(C_2C_1^{-1} + \Phi_2\Phi_1^{-1}\right)^{-1} C_2C_1^{-1} \qquad (13a) \\ S_{12} &= 2\left(C_1C_2^{-1} + \Phi_1\Phi_2^{-1}\right)^{-1} \qquad (13b) \\ S_{21} &= 2\left(C_2C_1^{-1} + \Phi_2\Phi_1^{-1}\right)^{-1} \qquad (13c) \\ S_{22} &= I - 2\left(C_1C_2^{-1} + \Phi_1\Phi_2^{-1}\right)^{-1} C_1C_2^{-1} \qquad (13d) \end{aligned}$$

where the C_i and Φ_i matrices represent the tangential magnetic and electric field distributions of the ith grating structure and I is the unit matrix of the same dimension. By using such scattering matrices combined with the corresponding propagation constants of the different expansion modes and applying the generalized scattering matrix approach [13], one can obtain the reflection and transmission coefficients of multilayered grating slabs of finite thicknesses.

3. EXTRACTION OF EQUIVALENT PARAMETERS

After determining the reflection and transmission coefficients of a multilayered grating slab, it is useful to obtain the parameters of an equivalent homogenous slab of the same thickness that has the same transmission and reflection coefficients. These equivalent parameters can be an appropriate method to understand the characteristics of the different resonances in the grating structures. This also can be a good tool for designing metamaterials with negative permittivity and/or negative permeability by using a grating slab. Transmission through a prism represents the most appropriate approach for characterizing DNG metamaterial [15]. However, the present analysis is based on a constant-thickness slab. Cheng and Ziolkowski [14] introduced a simple approach based on an equivalent T network to extract the equivalent parameters in closed forms for a finite-thickness slab from its scattering parameters. However, their approach is limited to very small thickness compared with the operating wavelength and to normal incidence. To generalize their approach we introduced an equivalent inverse problem, which can be presented as an optimization problem as shown in Fig. 2. The reflection and transmission coefficients of the equivalent homogenous slab are obtained in closed forms [16]. Any simple optimization technique or minimum-search can be used for obtaining the equivalent parameters that minimize the corresponding error function.

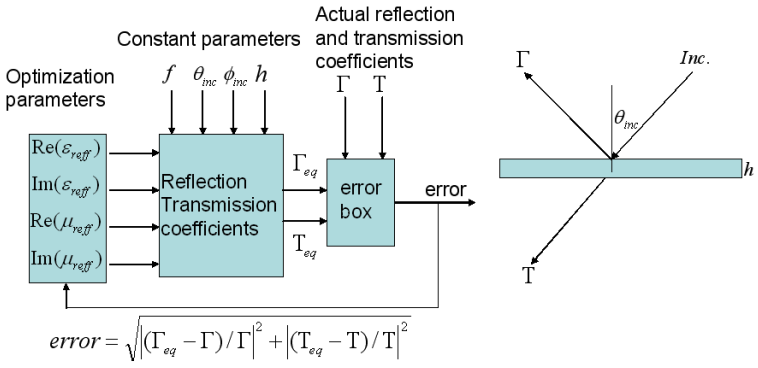

Figure 2. Block diagram of equivalent parameters extraction technique.

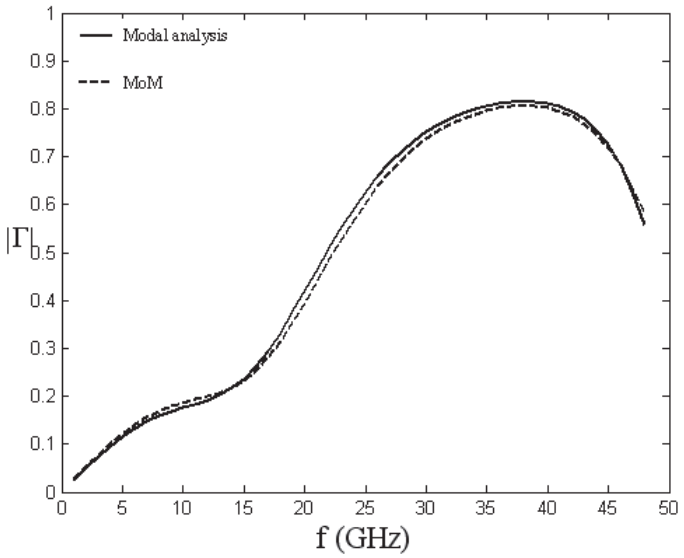

Figure 3. Reflection of a 2-D magneto-dielectric grating slab embedded between two dielectric slabs. The parameters of the grating slab are $D_x = D_y = 2\,\text{mm}$, $l_{x1} = l_{y1} = 1\,\text{mm}$, $x_{01} = y_{01} = 10\,\text{mm}$, $h = 2\,\text{mm}$, $\varepsilon_{rb} = 1$, $\mu_{rb} = 1$, $\varepsilon_{r1} = 2$ and $\mu_{r1} = 4$. The thickness of each dielectric slab is 1 mm. The dielectric constants of the upper and the lower slabs are 2.2 and 4, respectively. The excitation is a TM oblique incident plane wave with $\theta_{inc} = 30^\circ$ and $\phi_{inc} = 60^\circ$.

4. RESULTS AND DISCUSSIONS

Different configurations of 2-D magneto-dielectric grating slabs are discussed in this section to show their main characteristics and equivalent parameters. Most of the following examples are solved by using only 49 expansion functions with $-3 \leq m,\ n \leq 3$ in Equation (4). However, for large differences between the parameters of the base slab and the implanted rods, it is preferred to use a larger number of expansion functions up to ($-9 \leq m,\ n \leq 9$) to obtain convergent solutions. To verify the validity of the present approach, a comparison between modal analysis and MoM solutions for calculating the reflection coefficient of a magneto-dielectric grating slab embedded between two homogeneous dielectric slabs for an obliquely incident TM waves is shown in Fig. 3. One can notice very good agreement between the two results. Another example is considered to verify the present analysis. As a self-consistency test,

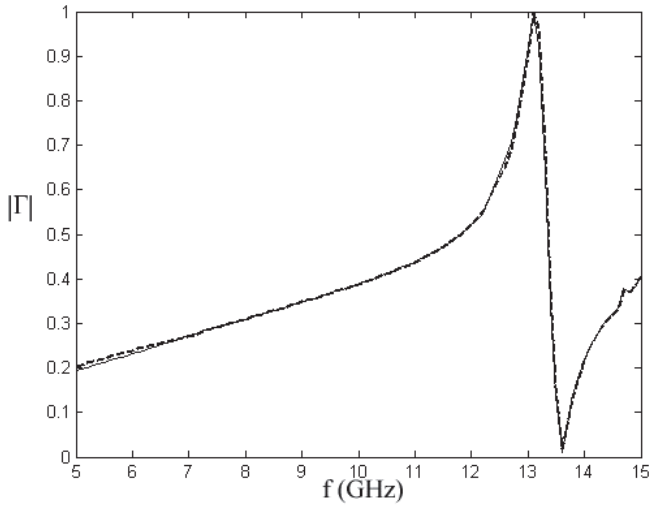

Figure 4. Magnitude of reflection coefficient of a 2-D grating slab due to normal incident plane wave with $D_x = D_y = 20\,\text{mm}$, $l_{x1} = 10\,\text{mm}$, $l_{y1} = 10\,\text{mm}$, $x_{01} = 10\,\text{mm}$, $y_{01} = 10\,\text{mm}$, $h = 2\,\text{mm}$; the solid line corresponds to $\varepsilon_{rb} = 2,\ \mu_{rb} = 1,\ \varepsilon_{r1} = 7$ and $\mu_{r1} = 1$, and the dashed line corresponds to the dual problem where $\varepsilon_{rb} = 1,\ \mu_{rb} = 2,\ \varepsilon_{r1} = 1$ and $\mu_{r1} = 7$.

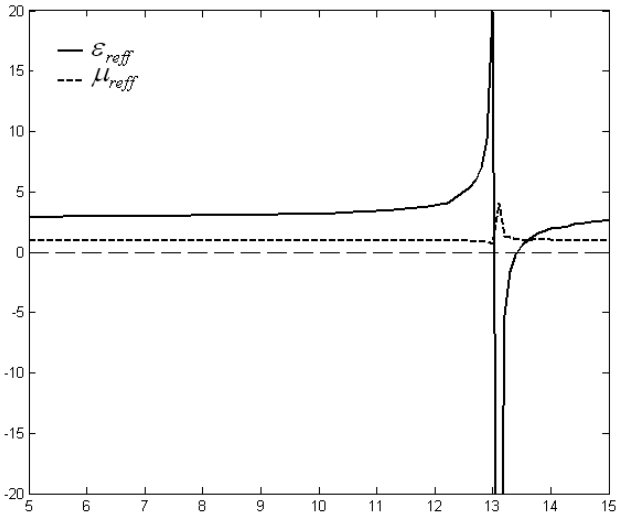

Figure 5. Equivalent parameters of the dielectric grating slab of Fig. 4; $\varepsilon_{rb} = 2,\ \mu_{rb} = 1,\ \varepsilon_{r1} = 7$ and $\mu_{r1} = 1$.

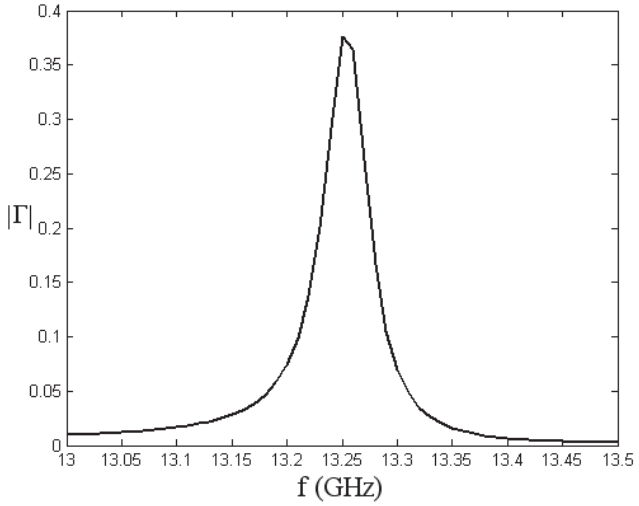

Figure 6. Magnitude of reflection coefficient of a 2-D grating slab due to normal incident plane wave. $D_x = D_y = 20\,\text{mm}$, $l_{x1} = 10\,\text{mm}$, $l_{y1} = 10\,\text{mm}$, $x_{01} = 10\,\text{mm}$, $y_{01} = 10\,\text{mm}$ and $h = 2\,\text{mm}$, $\varepsilon_{rb} = 2$, $\mu_{rb} = 2$, $\varepsilon_{r1} = 3$ and $\mu_{r1} = 3$.

the reflection coefficients of the above dielectric grating structure (Fig. 3) are computed under normal incidence and compared with its dual grating slab. As expected, the structure and its dual give the same reflection coefficients as shown in Fig. 4. Fig. 5 shows the equivalent material parameters of the dielectric grating structure of Fig. 4. It is observed that the increase of the reflection coefficient in this case is effectively due to the increase in the stored electrical energy in the grating structure, which corresponds to the increase in the equivalent permittivity. Around the resonance frequency, the dielectric slab is converted from highly positive permittivity to a highly negative permittivity. Then, the highly negative permittivity is increased to be positive as the frequency increases farther. On the other hand, the relative permeability is increased as a sharp peak around the center of the negative permittivity. However, this peak is much less than the peak of the relative permittivity. In this band, the total stored energy is converted to magnetic energy. At higher frequencies, the equivalent relative permittivity is converted back gradually to positive value. This explains the reflection minimum that just follows the resonance of the grating structure in this case. Similarly, one can explain the resonance behavior of the magnetic grating slab. In the case of magneto-dielectric

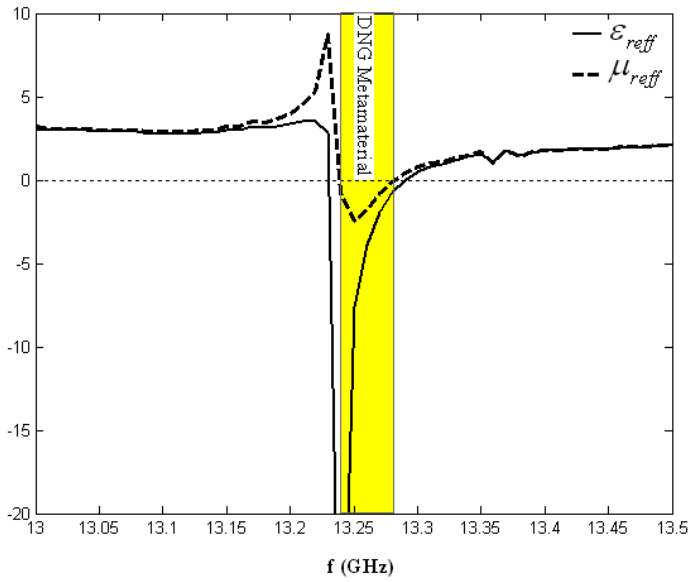

Figure 7. Equivalent relative permittivity and permeability of the grating slab of Fig. 6. Shaded region corresponds to DNG metamaterial.

grating structures with $\varepsilon_{r1} > \mu_{r1}$ and $\varepsilon_{rb} > \mu_{rb}$ it is found that such structures have quite similar properties to dielectric grating slabs, while magneto-dielectric grating structures with $\mu_{r1} > \varepsilon_{r1}$ and $\mu_{rb} > \varepsilon_{rb}$ have quite similar properties to magnetic grating slabs. On the other hand, a magneto-dielectric grating can be tailored for a special case where both the base slab and the implanted rods have the characteristic impedance of free space and have different propagation constants such that $\varepsilon_{r1} = \mu_{r1}$ and $\varepsilon_{rb} = \mu_{rb}$ where $\varepsilon_{r1} \neq \varepsilon_{rb}$. In this case the reflection coefficient of such grating structure due to normal incidence is characterized by a narrow band resonance surrounded by very low reflection coefficient as shown in Fig. 6 for a 2-D grating slab with the following parameters; $D_x = D_y = 20\,\text{mm}$, $l_{x1} = 10\,\text{mm}$, $l_{y1} = 10\,\text{mm}$, $x_{01} = 10\,\text{mm}$, $y_{01} = 10\,\text{mm}$, $h = 2\,\text{mm}$, $\varepsilon_{rb} = 2$, $\mu_{rb} = 2$, $\varepsilon_{r1} = 3$ and $\mu_{r1} = 3$. The equivalent parameters for such a grating structure are shown in Fig. 7. It can be noticed that the resonance in this case is mainly due to stored magnetic energy. It can also be noted that both the relative permittivity and relative permeability turn simultaneously into negative values in a very narrow band to form an equivalent DNG slab. Fig. 8 shows the reflection coefficients of the same magneto-dielectric grating slab for TE and TM obliquely

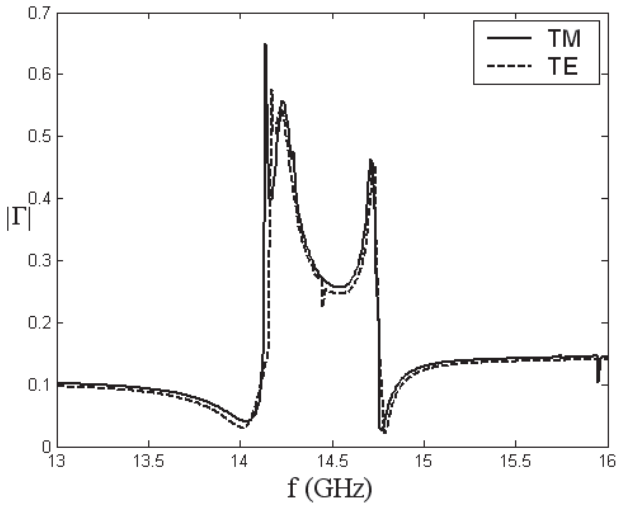

Figure 8. Magnitude of TE and TM reflection coefficients of a 2-D grating slab due to an obliquely incident plane wave; $\theta_{inc} = 30°$ and $\phi_{inc} = 0°$. The parameters of the grating structure are the same as for Fig. 6.

incident waves where $\theta_{inc} = 30°$ and $\phi_{inc} = 0°$. One may notice that the resonance bandwidth is increased slightly as the interaction between the two nearby resonances and the value of the background reflection surrounding the resonance are also increased. Due to the symmetry of this grating structure and the duality effects of the relative permittivity and relative permeability on TM and TE waves, the TE and TM responses in this case are identical. The slight difference shown between the results can be related to the numerical accuracy of solving the combined eigenvalue problems. Fig. 9 shows the equivalent parameters in this case for both TM and TE incident waves. Note that the total resonance is composed of two resonances. For the TM case these resonances are due to large stored electric energy followed by large stored magnetic energy, while the reverse behavior applies for the TE case. One may also note that the equivalent parameters do not turn simultaneously into negative values. This means that the DNG property, which is found with the normal plane wave incidence in a narrow band, disappears for the oblique incidence case. Fig. 10 shows the effect of increasing the values of ε_{r1} and μ_{r1} for the case of normal incidence. A bandwidth increase is noted in this case. The equivalent parameters for Fig. 10 case are shown in Fig. 11 providing a wider bandwidth for the DNG property. By comparing Fig. 11 with Fig. 7 it

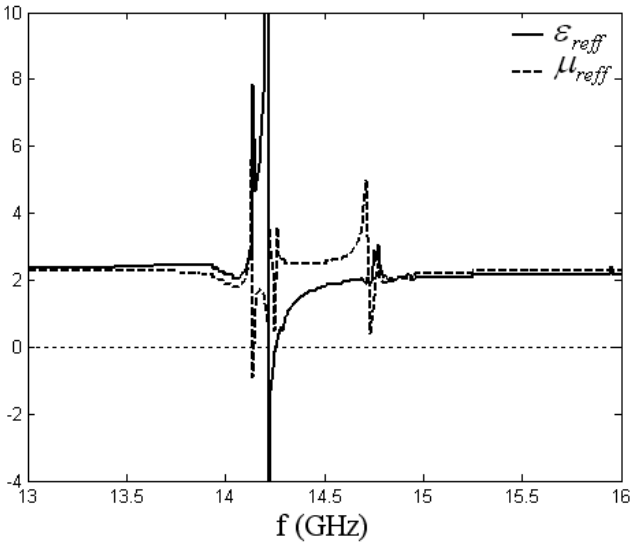

Figure 9a. Equivalent relative permittivity and permeability of the grating slab of Fig. 8 for TM incident wave.

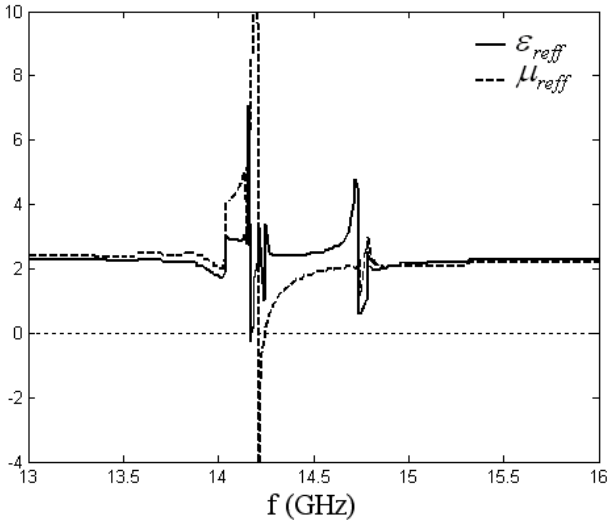

Figure 9b. Equivalent relative permittivity and permeability of the grating slab of Fig. 8 for TE incident wave.

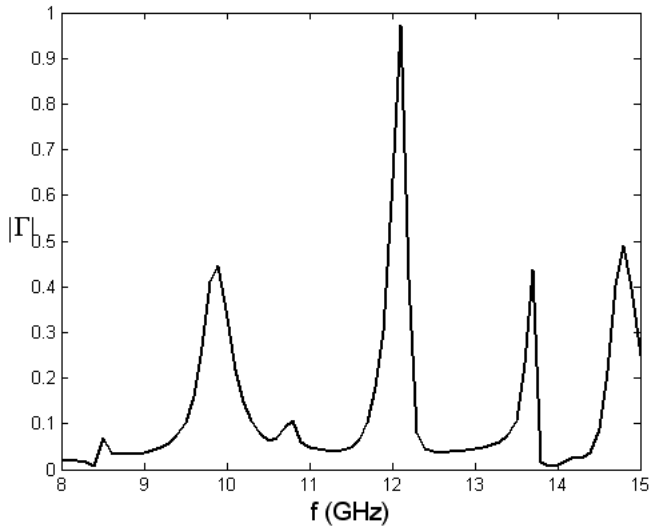

Figure 10. Magnitude of reflection coefficient of a 2-D grating slab due to normally incident plane wave. $D_x = D_y = 20\,\text{mm}$, $l_{x1} = 10\,\text{mm}$, $l_{y1} = 10\,\text{mm}$, $x_{01} = 10\,\text{mm}$, $y_{01} = 10\,\text{mm}$ and $h = 2\,\text{mm}$, $\varepsilon_{rb} = 2$, $\mu_{rb} = 2$, $\varepsilon_{r1} = 7$ and $\mu_{r1} = 7$.

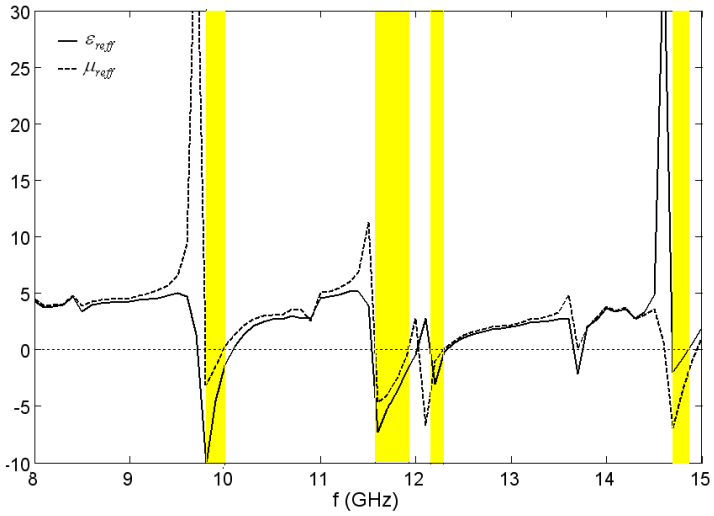

Figure 11. Equivalent relative permittivity and permeability of the grating slab of Fig. 8 for TE incident wave.

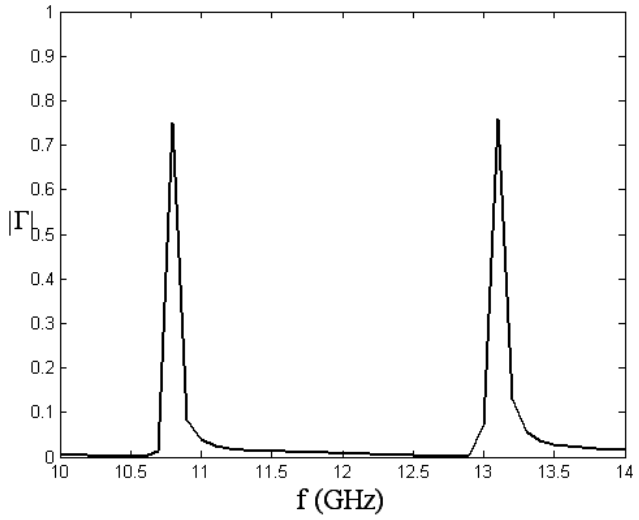

Figure 12. Magnitude of reflection coefficient of a 2-D grating slab due to normally incident plane wave. $D_x = D_y = 20\,\text{mm}$, $l_{x1} = 5\,\text{mm}$, $l_{y1} = 5\,\text{mm}$, $x_{01} = 10\,\text{mm}$, $y_{01} = 10\,\text{mm}$ and $h = 2\,\text{mm}$, $\varepsilon_{rb} = 4$, $\mu_{rb} = 4$, $\varepsilon_{r1} = 1$ and $\mu_{r1} = 1$.

can be noted that the magnitude of the equivalent parameters in the DNG region is decreased by increasing ε_{r1} and μ_{r1}. It is also observed that the DNG properties disappear as ε_{r1} and μ_{r1} increase.

In the previous examples the relative permittivity and permeability of the implanted rods are greater than the corresponding ones of the base slab. Fig. 12 shows another example where the implanted rods are free space holes inside a magneto-dielectric slab. The resonance behavior in this case due to normal incidence is quite similar to the previous case shown in Fig. 6. However, the equivalent parameters shown in Fig. 13 for this case present another explanation for the resonance characteristics, where either the relative permittivity or the relative permeability becomes negative but not both of them simultaneously. From these two examples, it can be concluded that the DNG property can be obtained only for implanted rods of relative permittivity and permeability greater than the corresponding ones of the supporting slab.

Figure 14 shows another special case where the values of the relative permittivity and relative permeability of the base slab and the implanted rods are interchanged such that $\varepsilon_{r1} = \mu_{rb}$ and $\varepsilon_{rb} = \mu_{r1}$. In this case the characteristic impedance of the base and the rods are

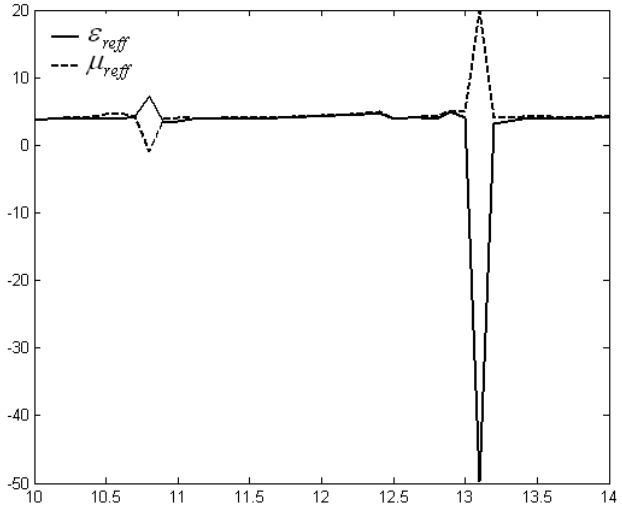

Figure 13. Equivalent relative permittivity and permeability of the grating slab of Fig. 12.

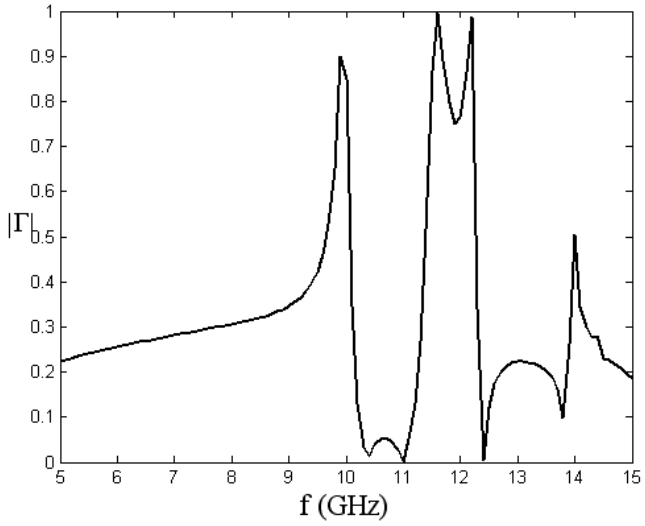

Figure 14. Magnitude of reflection coefficient of a 2-D grating slab due to normal incident plane wave. $D_x = D_y = 20\,\text{mm}$, $l_{x1} = 10\,\text{mm}$, $l_{y1} = 10\,\text{mm}$, $x_{01} = 10\,\text{mm}$, $y_{01} = 10\,\text{mm}$ and $h = 2\,\text{mm}$, $\varepsilon_{rb} = 2$, $\mu_{rb} = 7$, $\varepsilon_{r1} = 7$ and $\mu_{r1} = 2$.

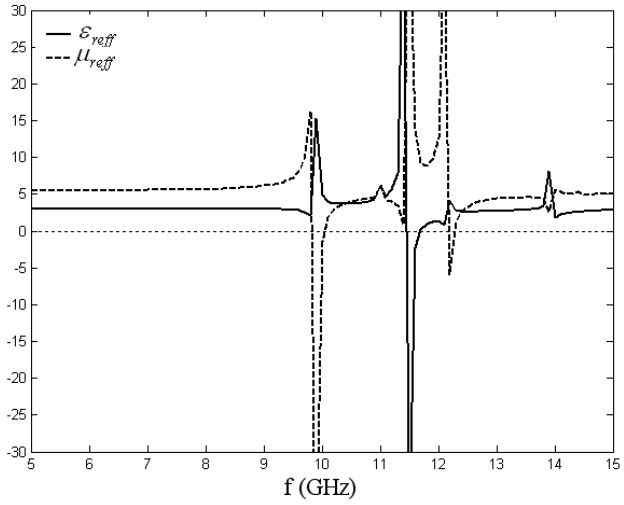

Figure 15. Equivalent relative permittivity and permeability of the grating slab of Fig. 14.

different but the wave propagation constant is the same. It can be noticed that the behavior of the reflection coefficient in this case for the lower frequency band is similar to the corresponding one of the dielectric or magnetic grating slab shown in Fig. 4. However, over the higher frequency band multiple closed resonances create a wide reflection band. The effective parameters of this grating structure are shown in Fig. 15. It can be noticed that this structure can be used to design either negative permittivity or negative permeability material but it cannot be used to design a DNG metamaterial slab.

5. CONCLUSION

Detailed modal analysis of a 2-D magneto-dielectric grating structure was discussed. This modal analysis combined with the generalized scattering matrix approach was used to study the reflection and transmission coefficients of different multilayered 2-D magneto-dielectric grating slabs. The accuracy of this modal analysis combined with the generalized scattering matrix approach was verified by comparison with MoM and verification of duality between dielectric and magnetic grating slabs. A general approach for extracting the equivalent parameters of a finite thickness slab based on its transmission and reflection coefficients for an arbitrary incidence plane wave was discussed. This approach was used to extract the equivalent

parameters of different magneto-dielectric grating slabs. It was found that a dielectric (magnetic) grating could be used to design a negative permittivity (permeability) slab. A magneto-dielectric grating with dominating variation in its relative permittivity was found to have similar behavior of dielectric grating slab and vise versa. It is also found that magneto-dielectric grating of $\varepsilon_{r1} = \mu_{r1}$ and $\varepsilon_{rb} = \mu_{rb}$ can be used to design a narrow band DNG for normal incidence if $\varepsilon_{r1} > \varepsilon_{rb}$. Such DNG bandwidth increased by increasing the difference between ε_{r1} and ε_{rb}. However, increasing this difference decreased the magnitude of the equivalent negative parameters. For larger differences between ε_{r1} and ε_{rb} the DNG could not be obtained. Also the DNG property could not be obtained by using a finite grating slab with oblique incidence. For a magneto-dielectric grating with, the resonance behavior is found to be equivalent to either negative permittivity or negative permeability but not both together. Another property of the magneto-dielectric grating with $\varepsilon_{r1} = \mu_{r1}$ and $\varepsilon_{rb} = \mu_{rb}$ was the narrow bandwidth resonances which were characterized by narrow band high reflection coefficients embedded between wideband low reflection coefficients. Another special case was discussed where the values of the relative permittivity and relative permeability of the base slab and the implanted rods were interchanged such that $\varepsilon_{r1} = \mu_{rb}$ and $\varepsilon_{rb} = \mu_{r1}$. The properties of such grating structures were found to be similar to the corresponding properties of magnetic or dielectric grating slabs. However, this grating structure was found also to have multi-resonances, which created a wider reflection bandwidth.

APPENDIX A.

For the special case where the transverse periodic cell of the grating is composed of rectangular rods, the relative permittivity and permeability as functions of transverse coordinates are given by

$$\begin{aligned}\varepsilon_r(x,y) &= \varepsilon_{rb} + \sum_{i=1}^{ND}[(\varepsilon_{ri}-\varepsilon_{rb})(H(x-x_{0i}+l_{xi}/2)-H(x-x_{0i}-l_{xi}/2)) \\ &\quad \times(H(y-y_{0i}+l_{yi}/2) - H(y-y_{0i}-l_{yi}/2))] \qquad \text{(A1a)} \\ \mu_r(x,y) &= \mu_{rb} + \sum_{i=1}^{ND}[(\mu_{ri}-\mu_{rb})(H(x-x_{0i}+l_{xi}/2)-H(x-x_{0i}-l_{xi}/2)) \\ &\quad \times(H(y-y_{0i}+l_{yi}/2) - H(y-y_{0i}-l_{yi}/2))] \qquad \text{(A1b)}\end{aligned}$$

where $H(x)$ is the Heaviside function, ε_{rb} and μ_{rb} are the relative permittivity and permeability of the base material, ε_{ri} and μ_{ri} are the relative permittivity and permeability of the ith rod, l_{xi} and l_{yi} are the

transverse dimensions of the ith rod, (x_{0i}, y_{0i}) is the transverse central location of the ith rod, and ND is the number of dielectric rods per unit cell. For this case, the matrix elements of Eq. (6) can be obtained in closed forms as follows

$$\begin{aligned}
L_{pq}^{TE/TE} &= \tilde{\beta}_p^2\delta_{pq} + k_0^2 R_0(k_{x(p)} - k_{x(q)}, k_{y(p)} - k_{y(q)}) \\
&\quad +(jk_{x(q)}\sin\phi_{inc} - jk_{y(q)}\cos\phi_{inc}) \\
&\quad \times(-R_{1x}(k_{x(p)} - k_{x(q)}, k_{y(p)} - k_{y(q)})\sin\phi_{inc} \\
&\quad +R_{1y}(k_{x(p)} - k_{x(q)}, k_{y(p)} - k_{y(q)})\cos\phi_{inc}) \\
&\quad -(jk_{x(p)}\cos\phi_{inc} + jk_{y(p)}\sin\phi_{inc}) \\
&\quad \times(Q_{1x}(k_{x(p)} - k_{x(q)}, k_{y(p)} - k_{y(q)})\cos\phi_{inc} \\
&\quad +Q_{1y}(k_{x(p)} - k_{x(q)}, k_{y(p)} - k_{y(q)})\sin\phi_{inc}) \qquad \text{(A2a)} \\
L_{pq}^{TM/TM} &= \tilde{\beta}_p^2\delta_{pq} + k_0^2 R_0(k_{x(p)} - k_{x(q)}, k_{y(p)} - k_{y(q)}) \\
&\quad +(jk_{x(q)}\cos\phi_{inc} + jk_{y(q)}\sin\phi_{inc}) \\
&\quad \times(-R_{1x}(k_{x(p)} - k_{x(q)}, k_{y(p)} - k_{y(q)})\cos\phi_{inc} \\
&\quad -R_{1y}(k_{x(p)} - k_{x(q)}, k_{y(p)} - k_{y(q)})\sin\phi_{inc}) \\
&\quad -(jk_{x(p)}\sin\phi_{inc} - jk_{y(p)}\cos\phi_{inc}) \\
&\quad \times(-Q_{1x}(k_{x(p)} - k_{x(q)}, k_{y(p)} - k_{y(q)})\sin\phi_{inc} \\
&\quad +Q_{1y}(k_{x(p)} - k_{x(q)}, k_{y(p)} - k_{y(q)})\cos\phi_{inc}) \qquad \text{(A2b)} \\
L_{pq}^{TE/TM} &= -(jk_{x(q)}\cos\phi_{inc} - jk_{y(q)}\sin\phi_{inc}) \\
&\quad \times(-R_{1x}(k_{x(p)} - k_{x(q)}, k_{y(p)} - k_{y(q)})\sin\phi_{inc} \\
&\quad +R_{1y}(k_{x(p)} - k_{x(q)}, k_{y(p)} - k_{y(q)})\cos\phi_{inc}) \\
&\quad -(jk_{x(p)}\cos\phi_{inc} + jk_{y(p)}\sin\phi_{inc}) \\
&\quad \times(-Q_{1x}(k_{x(p)} - k_{x(q)}, k_{y(p)} - k_{y(q)})\sin\phi_{inc} \\
&\quad +Q_{1y}(k_{x(p)} - k_{x(q)}, k_{y(p)} - k_{y(q)})\cos\phi_{inc}) \qquad \text{(A2c)} \\
L_{pq}^{TM/TE} &= -(-jk_{x(q)}\sin\phi_{inc} + jk_{y(q)}\cos\phi_{inc}) \\
&\quad \times(R_{1x}(k_{x(p)} - k_{x(q)}, k_{y(p)} - k_{y(q)})\cos\phi_{inc} \\
&\quad +R_{1y}(k_{x(p)} - k_{x(q)}, k_{y(p)} - k_{y(q)})\sin\phi_{inc}) \\
&\quad -(-jk_{x(p)}\sin\phi_{inc} + jk_{y(p)}\cos\phi_{inc}) \\
&\quad \times(Q_{1x}(k_{x(p)} - k_{x(q)}, k_{y(p)} - k_{y(q)})\cos\phi_{inc} \\
&\quad +Q_{1y}(k_{x(p)} - k_{x(q)}, k_{y(p)} - k_{y(q)})\sin\phi_{inc}) \qquad \text{(A2d)}
\end{aligned}$$

where

$$\tilde{\beta}_p = \sqrt{\varepsilon_{rb}k_0^2 - k_{x(p)}^2 - k_{y(p)}^2} \qquad \text{(A3a)}$$

$$R_0(k_x,k_y) = \frac{1}{D_xD_y}\sum_{i=1}^{ND} 4(\varepsilon_{ri}\mu_{ri}-\varepsilon_{rb}\mu_{rb})\frac{\sin(k_xl_{xi}/2)}{k_x} \times\frac{\sin(k_yl_{yi}/2)}{k_y}e^{j(k_xx_{0i}+k_yy_{0i})} \quad \text{(A3b)}$$

$$R_{1x}(k_x,k_y) = \frac{1}{D_xD_y}\sum_{i=1}^{ND} 8j\frac{(\varepsilon_{ri}-\varepsilon_{rb})}{(\varepsilon_{ri}+\varepsilon_{rb})}\sin(k_xl_{xi}/2) \times\frac{\sin(k_yl_{yi}/2)}{k_y}e^{j(k_xx_{0i}+k_yy_{0i})} \quad \text{(A3c)}$$

$$R_{1y}(k_x,k_y) = \frac{1}{D_xD_y}\sum_{i=1}^{ND} 8j\frac{(\varepsilon_{ri}-\varepsilon_{rb})}{(\varepsilon_{ri}+\varepsilon_{rb})}\frac{\sin(k_xl_{xi}/2)}{k_x} \times\sin(k_yl_{yi}/2)e^{j(k_xx_{0i}+k_yy_{0i})} \quad \text{(A3d)}$$

$$Q_{1x}(k_x,k_y) = \frac{1}{D_xD_y}\sum_{i=1}^{ND} 8j\frac{(\mu_{ri}-\mu_{rb})}{(\mu_{ri}+\mu_{rb})}\sin(k_xl_{xi}/2) \times\frac{\sin(k_yl_{yi}/2)}{k_y}e^{j(k_xx_{0i}+k_yy_{0i})} \quad \text{(A3e)}$$

$$Q_{1y}(k_x,k_y) = \frac{1}{D_xD_y}\sum_{i=1}^{ND} 8j\frac{(\mu_{ri}-\mu_{rb})}{(\mu_{ri}+\mu_{rb})}\frac{\sin(k_xl_{xi}/2)}{k_x} \times\sin(k_yl_{yi}/2)e^{j(k_xx_{0i}+k_yy_{0i})} \quad \text{(A3f)}$$

REFERENCES

1. Yang, H. Y. D., R. Diaz, and N. G. Alexopoulos, "Reflection and transmission of waves from multilayer structures with planar-implanted periodic material blocks," *J. Opt. Soc. Amer. B*, Vol. 14, 2513–2521, Oct. 1997.
2. Yachin, V. V. and N. V. Ryazantseva, "The scattering of electromagnetic waves by rectangular-cell double-periodic magnetodielectric gratings," *Microwave Optical Technology Letters*, Vol. 23, No. 3, 177–183, Nov. 1999.
3. Holloway, C. L., E. F. Kuester, J. K.-Jarvis, and P. Kabos, "A double negative (DNG) composite medium composed of magnetodielectric spherical particles embedded in a matrix," *IEEE Trans. Antennas Propagat.*, Vol. 51, No. 10, 2596–2603, Oct. 2003.

4. Alu, A. and N. Engheta, "Pairing an epsilon-negative slab with a mu-negative slab: Resonance, anomalous tunneling and transparency," *IEEE Trans. Antennas Propagat.*, Vol. 51, No. 10, 2558–2571, October 2003.
5. Ziolkowski, R. W. and D. Kipple, "Application of double negative materials to increase the power radiated by electrically small antennas," *IEEE Trans. Antennas Propagat.*, Vol. 51, No. 10, 2626–2640, Oct. 2003.
6. Taflove, A. and S. C. Hagness, *Computational Electrodynamics: The Finite-Difference Time-Domain Method*, 2nd edition, Artech House, Norwood, MA, 2000.
7. Pelosi, G., R. Coccioli, and S. Selleri, *Quick Finite Element Method for Electromagnetic Waves*, Artech House, 1998.
8. Coves, A., B. Gimeno, A. A. San Blas, A. Vidal, V. E. Boria, and M. V. Andres, "Three-diemensional scattering of dielectric gratings under plane-wave excitation," *IEEE Antennas and Wireless Propagation Letters*, Vol. 2, 215–218, 2003.
9. Coves, A., B. Gimeno, J. Gil, M. V. Andres, A. A. San Blas, and V. E. Boria, "Full-wave analysis of dielectric frequency-selective surfaces using vectorial modal method," *IEEE Trans. Antennas Propagat.*, Vol. 52, 2091–2099, Aug. 2004.
10. Jarem, J. M. and P. P. Banerjee, *Computational Methods for Electromagnetic and Optical Systems*, Marcel Dekker, Inc., 2000.
11. Peng, S. T., T. Tamir, and H. L. Bertoni, "Theory of periodic dielectric waveguides," *IEEE Trans. Microwave Theory Techniques*, Vol. 23, 123–133, Jan. 1975.
12. Peng, S. T., "Rigorous formulation of scattering and guidance by dielectric grating waveguides: General case of oblique incidence," *J. Opt. Soc. Amer. A*, Vol. 6, No. 12, 1869–1883, Dec. 1989.
13. Mittra, R., C. H. Chan, and T. Cwik, "Techniques for analyzing frequency selective surfaces-a review," *Proc. IEEE*, Vol. 76, 1593–1615, Dec. 1988.
14. Cheng, C.-Y. and R. W. Ziolkowski, "Tailoring double-negative metamaterial responses to achieve anomalous propagation effects along microstrip transmission lines," *IEEE Transactions on Microwave Theory and Techniques*, Vol. 51, No. 12, 2306–2314, Dec. 2003.
15. Ran, L., J. Huangfu, H. Chen, X. Zhang, K. Cheng, T. M. Grzegorczyk, and J. A. Kong, "Experimental study on several left-handed metamaterials," *Progress In Electromagnetics Research*, PIER 51, 249–279, 2005.

16. Chew, W. C., *Waves and Fields in Inhomogeneous Media*, IEEE Press, 1995.
17. Attiya, A. M. and A. Kishk, "Modal analysis of two-dimensional dielectric grating slab excited by an obliquely incident plane wave," *Progress In Electromagnetics Research*, PIER 60, 221–243, 2006.